American Mineralogist, Volume 94, pages 1039–1044, 2009

Thermoelasticity of ε-FeSi to 8 GPa and 1273 K

Matthew L. Whitaker,[1,2,*] Wei Liu,[2] Qiong Liu,[2] Liping Wang,[2] and Baosheng Li[2]

[1]Department of Geosciences, Stony Brook University, Stony Brook, New York 11794-2100, U.S.A.
[2]Mineral Physics Institute, Stony Brook University, Stony Brook, New York 11794-2100, U.S.A.

Abstract

The elastic properties of ε-FeSi were investigated at high temperature and pressure using a combination of ultrasonic interferometry and synchrotron radiation up to 8 GPa and 1273 K. The unit-cell volumes and sound velocity data were fit to third-order finite-strain equations with adiabatic temperature conversions to maintain a thermodynamically internally consistent data set. The adiabatic zero-pressure bulk and shear moduli and their first pressure and temperature derivatives were obtained from this fitting: K_{S0} = 168.9(7) GPa, G_0 = 116.5(3) GPa, K_{S0}' = 6.6(2), G_0' = 2.9(1), $(\partial K_{S0}/\partial T)_P$ = –0.023(1) GPa/K, $(\partial G_0/\partial T)_P$ = –0.030(1) GPa/K. This study presents the first complete thermodynamically consistent set of elastic moduli and their temperature and pressure derivatives.

Keywords: Ultrasonic interferometry, equation of state, iron silicide, elastic properties, high pressure, high temperature

Introduction

Many previous investigations have been directed at unraveling the possible composition of the Earth's core (i.e., McDonough and Sun 1995). It has long been accepted that the core is made up of a predominantly metallic iron, or iron-nickel, alloy; however, several studies have shown that both metallic Fe and Fe-Ni alone are too dense to be the sole element in the Earth's core, particularly the solid inner core (i.e., Dziewonsky and Anderson 1981; Jephcoat and Olson 1987; Mao et al. 1998). These studies, as well as several others, suggest that there must be some amount of some light element(s) in the core.

Silicon has been strongly suggested by previous studies to be a possible light-element constituent of the Earth's core based on both density and velocity data (Badro et al. 2007), as well as on isotopic and geochemical data (Georg et al. 2007). To assess the possibility of Si as a constituent of the core, physical properties of Si-bearing iron phases under extreme conditions must be determined. This study is part of a continuing effort begun in Whitaker et al. (2008) that is designed to address this issue by studying ε-FeSi at high pressure and high temperature.

Under ambient conditions, FeSi occurs as ε-FeSi, which is a cubic material (B20 structure) in which the coordination numbers of both Si and Fe are seven (Pauling and Soldate 1948), and has a modified NaCl structure wherein the silicon and iron atoms are displaced along the [111] directions (Knittle and Williams 1995). Considerable debate exists over the behavior and physical properties of ε-FeSi under extreme conditions in spite of several previous studies that have been conducted on this material (Guyot et al. 1997; Knittle and Williams 1995; Lin et al. 2003; Sarrao et al. 1994; Whitaker et al. 2008; Wood et al. 1995). Some of this debate was clarified by Whitaker et al. (2008) in a study on the high-pressure elasticity of ε-FeSi at ambient temperatures, which presented the first complete data set on the bulk and shear moduli and their first pressure derivatives. However, despite all of these previous experimental studies on fersilicite, there is no available data on the temperature dependence of the elastic properties of this phase. This study sets out to determine the elastic properties of ε-FeSi in situ under high pressure and temperature, and examines the pressure and temperature dependence of these properties by using ultrasonic interferometry combined with synchrotron-based X-ray diffraction and X-radiographic imaging.

* E-mail: matt@mattwhitaker.net

Experimental methods

The starting material for this study was powdered FeSi (99.9% pure) purchased from Alfa Aesar. X-ray powder diffraction of this material indicated that the powder was homogeneous and pure ε-FeSi. The bulk powder was then hand-ground with an agate mortar and pestle for ~30 min, resulting in a fine powder with an average grain size on the order of a few micrometers. This fine powder was loaded into a gold capsule and dried at 150 °C for 2 h, after which the capsule was pressure-sealed so as to prevent moisture adsorption. This capsule was then placed into the standard COMPRES 14/8 octahedral cell assembly for a hot-pressing experiment. The sample was sintered at 700 °C and 7 GPa in a Kawai-type 1000 ton uniaxial split-cylinder apparatus for exactly 1 h before temperature quenching and decompression. Visual inspection, X-ray diffraction, and SEM analysis of the finished run products all suggest that no oxidation of the FeSi occured at any step during these sample preparation procedures.

The resulting sintered cylindrical sample was then analyzed at beamline X17B2 at the National Synchrotron Light Source (NSLS) at Brookhaven National Laboratory (BNL) to check for heterogeneity in grain size and/or composition. X-ray diffraction patterns of the sample were collected at a series of points while under ambient conditions by changing its position in the beam laterally and vertically; the diffracted X-rays were collected by four detectors (two aligned vertically and two horizontally) positioned at χ = 0°, 90°, 180°, and 270° (Fig. 1). The diffraction patterns recorded by the horizontal (3 and 4 in Fig. 1) and vertical detectors (1 and 2 in Fig. 1) were virtually identical for each point analyzed, and all points analyzed gave similar diffraction patterns to those in Figure 1; this indicates that there was no detectable preferred orientation of the grains in the sample, and in conjunction with SEM analyses of the sample, suggests a uniform grain size and a pure and homogeneous ε-FeSi composition. Small unlabelled peaks in these diffraction patterns were either sample peaks not used for refinement or parasitic peaks from the surrounding cell assembly.

The in situ ultrasonic and X-ray experiment was conducted in the cubic-anvil apparatus (SAM85) installed at NSLS beamline X17B2. A schematic diagram and detailed description of the experimental setup can be found in Whitaker et al. (2008). The sample, surrounded by a BN sleeve and the NaCl:BN 10:1 mixture, was first compressed to the maximum oil pressure of 60 tons while at room *T*, after which it was heated to the maximum temperature of 1273 K; this resulted in a pressure decrease from 12 to 8 GPa as the cell assembly relaxed and flowed at high *T*. Data were collected at this maximum temperature, and in 200 K intervals on the way down to room *T*, after which seven additional heating and cooling cycles were conducted at about a 0.5–1.0 GPa interval in pressure to provide a dense coverage in *P-T* space. At all *P-T* conditions, the ultrasonic data, an X-radiographic image, and an X-ray diffraction pattern of the FeSi sample were obtained.

The ultrasonic interferometry measurements were conducted with a dual-mode $LiNbO_3$ transducer (10° Y-cut) capable of generating and receiving a range of frequencies from 20 to 70 MHz. This allows us to determine P and S wave travel times simultaneously with a deviation of ~0.4 ns for S waves and ~0.2 ns for P waves. The transfer function method (Li et al. 2002) is used to record the acoustic responses of the cell assembly in the aforementioned frequency range; the monochromatic waveform data are then extracted from these measurements offline following the experiment, and the pulse echo overlap (PEO) technique is used to determine the two-way travel times of the P and S waves traveling through the sample. The P and S wave travel times were obtained at 60 and 35 MHz, respectively, in this study to maximize the signal-to-noise ratio. More information on these ultrasonic measurements and the processing of this data can be found in Li et al. (2002, 2004).

X-ray diffraction patterns were collected with a solid-state Ge detector in energy-dispersive mode. The incident X-ray beam was collimated to 100 × 100 μm, and the 2θ angle was calibrated at 6.495° for this experiment. The CCD camera recorded snapshots of the cell assembly at each desired set of temperature and pressure conditions. This X-radiographic imaging gives a direct means of measuring the sample length during the experiment; by measuring the absolute length of the sample and comparing it to the length of the sample in pixels at the end of the experiments, a pixel-to-length ratio can be determined and applied to every image collected, thereby giving the absolute length of the sample at all *P-T* conditions. The precision of this direct image measurement of sample length has been shown to be ~0.2–0.4% (Li et al. 2004). From the sample lengths and travel times, the P and S wave velocities can be directly obtained.

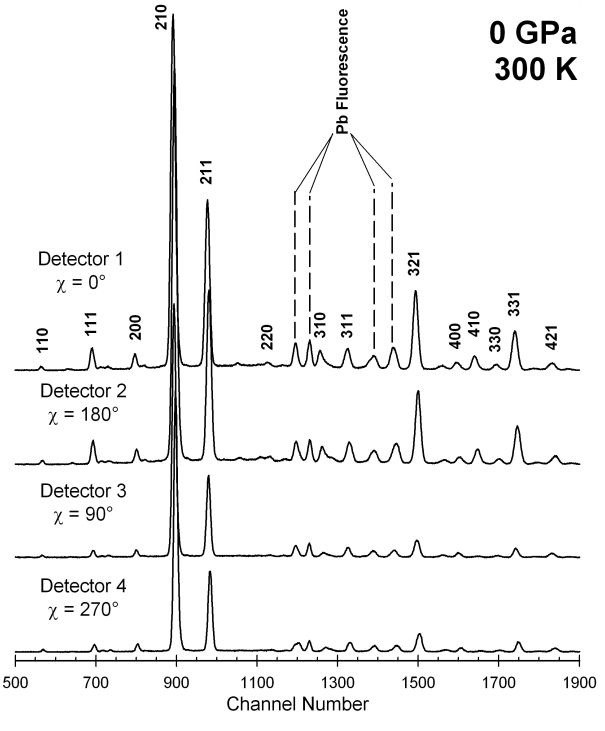

FIGURE 1. X-ray diffraction patterns of the ε-FeSi sample taken by each of the four detectors at ambient pressure and temperature. Orientation of the detector is shown for each pattern. Intensities normalized to highest peak intensity (Detector 2) for comparison between patterns. Slight shifts in peak position between detectors are caused by differences in calibration angle for each detector. Peaks are labeled with their *hkl* values, and Pb fluorescence peaks are shown for reference. Only peaks used in cell refinement are labeled.

DATA PROCESSING

The shear ($G = \rho v_S^2$) and adiabatic bulk ($K_S = \rho v_P^2 - 4G/3$) moduli at high pressures and temperatures are obtained directly from the densities and acoustic velocities. The density (ρ) and velocity (v_P, v_S) data are simultaneously fit to the third-order finite strain equations (i.e., Davies and Dziewonski 1975):

$$\rho v_P^2 = (1-2\varepsilon)^{5/2}(L_1 + L_2\varepsilon) \quad (1)$$

$$\rho v_S^2 = (1-2\varepsilon)^{5/2}(M_1 + M_2\varepsilon) \quad (2)$$

where the volume strain on the sample (ε) is given by

$$\varepsilon = \frac{1-(V_0/V)^{2/3}}{2}. \quad (3)$$

The adiabatic bulk and shear moduli and their isothermal pressure derivatives $\{K_{S(0,300)}; K_{S(0,300)}' = [\partial K_{S(0,300)}/\partial P]_T; G_{(0,300)}; G_{(0,300)}' = [\partial G_{(0,300)}/\partial P]_T\}$ are related to the fitting coefficients through the following equations:

$$M_1 = G \quad (4)$$

$$M_2 = 5G - 3K_S G' \quad (5)$$

$$L_1 = K_S + \frac{4G}{3} \quad (6)$$

$$L_2 = 5L_1 - 3K_S\left(K_S' + \frac{4G'}{3}\right) \quad (7)$$

The temperature derivatives of the elastic moduli $\{[\partial K_{S(0,300)}/\partial T]_P; [\partial G_{(0,300)}/\partial T]_P\}$ were obtained by fitting all of the data at high temperature and high pressure. To do this, the entire data set was fitted to Equations 1–7 along individual isentropes, assuming the pressure at each data point was raised along an adiabatic path from zero pressure with different foot temperatures; in this way, we account for the fact that the acoustic response of the sample is measured adiabatically, while the experiment is conducted isothermally. The adiabatic foot temperature (T_0) for each data point, and the thermoelastic properties at zero pressure and T_0, are related to their values at zero pressure and room temperature via the following equations:

$$\left(\frac{\partial T}{\partial P}\right)_S = \frac{\gamma_{(0,T0)} T_0}{K_S} \quad (8)$$

$$\rho_{0,T_0} = \rho_{0,300} e^{-\int \alpha dT_0} \quad (9)$$

$$K_{S(0,T_0)} = K_{S(0,300)} + (T_0 - 300)\left(\frac{\partial K_S}{\partial T}\right)_P \quad (10)$$

$$G_{(0,T_0)} = G_{(0,300)} + (T_0 - 300)\left(\frac{\partial G}{\partial T}\right)_P \quad (11)$$

$$K'_{SS(0,T_0)} = \left(K'_{S(0,300)} + \left(T_0 - 300\right)\left(\frac{\partial^2 K_S}{\partial P \partial T}\right)_P \right) + \left(\frac{\partial K_S}{\partial T}\right)_P \left(\frac{\gamma T_0}{K_S}\right) \quad (12)$$

$$G'_{S(0,T_0)} = \left(G'_{S(0,300)} + \left(T_0 - 300\right)\left(\frac{\partial^2 G_S}{\partial P \partial T}\right)_P \right) + \left(\frac{\partial G}{\partial T}\right)_P \left(\frac{\gamma T_0}{K_S}\right) \quad (13)$$

where α is the thermal expansion coefficient ($\alpha = a + bT + cT^2$). More details about the data analysis procedures can be found elsewhere (i.e., Li and Zhang 2005; Liu et al. 2005). It should be noted here that in the current calculations, the Grüneisen parameter (γ_0) used is 2.33, and for the coefficients in the thermal expansion term, the values of $a = 3.75 \times 10^{-5}$, $b = 1.40 \times 10^{-8}$, and $c = 0$ are used (Vocadlo et al. 2002). In conducting all of these calculations, the assumptions that $\rho\gamma$ = constant and that the cross-derivatives $[(\partial^2 K_S/\partial P \partial T)_P$ and $(\partial^2 G/\partial P \partial T)_P]$ are equal to zero are employed. The pressure on the sample can then be concurrently calculated from these fitted elastic parameters (Eq. 14), without relying on an external pressure standard.

$$P = -\left(1 - 2\varepsilon\right)^{5/2}\left(3K_{S(0,T_0)}\varepsilon + \left(\frac{\left(36K_{S(0,T_0)} - 9K_{S(0,T_0)}K'_{SS(0,T_0)}\right)\varepsilon^2}{2}\right)\right) \quad (14)$$

The pressures calculated in this manner are given in Table 1 and are used in all subsequent figures and discussion.

Results and discussion

The X-ray diffraction patterns of the sample collected throughout the experiment indicated that the sample remained in the cubic B20 structure over all *P-T* conditions explored. The cell refinements were conducted in space group $P2_13$. A total of 9–13 diffraction lines were used in the cell refinement of the ε-FeSi diffraction patterns, depending on the peak intensities, pressure, and interference from fluorescence peaks. Unit-cell volumes obtained via cell refinement are given in Table 1 and have a relative standard deviation of less than 0.05%. The unit-cell volume at ambient conditions (V_0) was found to be 90.45(3) Å^3, which is slightly higher than, but comparable with, those of previous studies (see Table 2). The density of the sample at each set of *P-T* conditions is derived using the calculated theoretical density and the unit-cell volumes obtained from the cell refinement.

In addition to monitoring the sample structure and cell volume throughout the experiment, the X-ray diffraction patterns also suggest that there was minimal deviatoric stress acting on the sample during the experiment, as the peaks did not show any significant signs of broadening (full-width at half maximum, FWHM). The diffraction patterns throughout the experiment suggest there were little to no discernable changes in grain size or orientation during the experiment; this is reaffirmed by SEM images taken both before and after the experiment that show no difference in grain size.

The compressional and shear wave velocities obtained from all eight heating/cooling cycles during the experiment are shown in Figure 2. As this figure shows, the data agree quite well with the values obtained from the fitting of this data set over the entire range of conditions explored. Figure 3 shows the elastic moduli determined for each set of pressure and temperature conditions during the experiment. These data also largely agree with the values obtained from the fitting of the entire data set. The acoustic velocities and the elastic moduli all show a steady increase with increasing pressure at a constant temperature, and a decrease in value with temperature at a given pressure, as is expected.

Using the finite-strain approach, a fit of the entire data set given in Table 1 gives the adiabatic zero-pressure bulk and shear moduli and their first pressure and temperature derivatives: K_{S0} = 168.9(7) GPa, G_0 = 116.5(3) GPa, K_{S0}' = 6.6(2), G_0' = 2.9(1), $(\partial K_{S0}/\partial T)_P$ = –0.023(1) GPa/K, $(\partial G_0/\partial T)_P$ = –0.030(1) GPa/K. A third-order finite-strain fit of just the data collected at room temperature yields K_{S0} = 169.3(8) GPa, G_0 = 116.3(4) GPa, K_{S0}' = 6.5(3), G_0' = 3.0(1) (Whitaker et al. 2008). There is very good agreement between the elastic properties obtained via fitting of the entire data set, and those obtained using only the room-temperature data set. It should be noted that in the current fitting, pressure is not included in the fitting procedure, and therefore the elastic moduli and their pressure derivatives obtained via this method are not dependent upon pressure measurements taken during the experiment or upon the pressure standard chosen and/or the accuracy of the pressure scale used.

Table 2 presents a comparison of the thermoelastic properties of ε-FeSi obtained from this study with those of previous experimental and theoretical studies on this material. The first thing to note in this table is that this study reports the first data on the temperature dependence of the elastic moduli, and a complete set of thermodynamically internally consistent elastic properties and their pressure and temperature derivatives.

The bulk modulus of this material determined via first-principles calculations are all significantly higher than that obtained from this study. This difference may arise from two main sources: the necessary assumptions used to conduct such calculations, and the fact that such calculations are most often conducted at 0 K, whereas the thermoelastic properties from this study are all determined at a reference temperature of 300 K. To accurately compare the adiabatic bulk modulus from this study with those of previous experimental studies, which are isothermal values, the relationship $K_S/K_T = (1 + \alpha\gamma T) \approx 1.03$ was used to convert our K_{S0} to K_{T0}, which yielded a value of 164.2 GPa. This falls at the lower end of the range of previously reported values of K_{T0} for ε-FeSi, which spanned from 160 to 209 GPa. The K_{T0}' obtained from this study is higher than those found in all previous studies, which ranged from 3.5 to 4.75. The first temperature derivative of the adiabatic bulk modulus obtained in this study [–0.023(1) GPa/K], when converted to an isothermal value [–0.039(1) GPa/K] compares very well with the value of –0.043 GPa/K obtained by Guyot et al. (1997). Our shear modulus is in excellent agreement with the data from the previous resonant ultrasound study, and there are no existing data on the temperature dependence of the elastic shear modulus to use in a comparison.

The differences between the elastic properties determined in previous studies and those obtained in this study arise from several sources. Most of the previous experimental studies (with the exception of the resonant ultrasound study conducted only at ambient pressure) were static compression studies, which used a secondary pressure standard as a measure of pressure, and either

TABLE 1. Experimental ultrasonic and X-ray results on ε-FeSi at high *P* and *T*

P (GPa)	*T* (K)	2*tp* (μs)	2*ts* (μs)	*L* (mm)	*V* (Å³)	ρ (g cm⁻³)	v_P (km/s)	v_S (km/s)	K_S (GPa)	*G* (GPa)
7.98	1273	0.2428	0.4304	0.9020	89.89(3)	6.210	7.43	4.19	197.5	109.0
7.45	1073	0.2384	0.4190	0.8934	89.44(4)	6.241	7.50	4.26	200.0	113.3
7.05	873	0.2356	0.4108	0.8895	88.93(3)	6.276	7.55	4.33	200.9	117.7
6.51	673	0.2336	0.4042	0.8889	88.50(3)	6.307	7.61	4.40	202.4	122.1
6.10	473	0.2316	0.3964	0.8872	88.03(3)	6.340	7.66	4.48	202.3	127.2
5.45	308	0.2292	0.3898	0.8856	87.80(3)	6.357	7.73	4.54	205.1	131.0
4.85	300	0.2302	0.3902	0.8857	88.05(3)	6.339	7.70	4.54	201.6	130.7
7.12	1273	0.2430	0.4288	0.8940	90.33(3)	6.179	7.36	4.17	191.5	107.4
6.72	1073	0.2392	0.4186	0.8880	89.81(3)	6.215	7.42	4.24	193.2	111.7
6.23	873	0.2370	0.4110	0.8854	89.32(4)	6.249	7.47	4.31	193.9	116.1
5.77	673	0.2350	0.4042	0.8838	88.85(4)	6.282	7.52	4.37	195.3	120.0
5.19	473	0.2328	0.3970	0.8829	88.44(4)	6.311	7.58	4.45	196.0	125.0
4.60	308	0.2306	0.3894	0.8813	88.18(4)	6.330	7.64	4.53	196.3	129.9
3.95	303	0.2316	0.3908	0.8825	88.46(5)	6.310	7.62	4.52	194.5	128.9
6.21	1073	0.2406	0.4198	0.8900	90.06(3)	6.198	7.40	4.24	190.8	111.4
5.68	873	0.2384	0.4128	0.8878	89.60(4)	6.230	7.45	4.30	192.2	115.2
5.15	673	0.2364	0.4062	0.8852	89.14(3)	6.262	7.49	4.36	192.6	119.0
4.51	473	0.2344	0.3994	0.8837	88.77(3)	6.288	7.54	4.43	192.9	123.4
3.98	308	0.2320	0.3916	0.8832	88.47(3)	6.309	7.61	4.51	194.3	128.3
3.23	304	0.2336	0.3936	0.8835	88.81(3)	6.285	7.56	4.49	190.3	126.7
5.53	1073	0.2430	0.4228	0.8913	90.43(3)	6.172	7.34	4.22	186.0	109.9
5.00	873	0.2406	0.4152	0.8877	89.94(4)	6.206	7.38	4.28	186.4	113.7
4.37	673	0.2384	0.4082	0.8866	89.53(4)	6.234	7.44	4.34	188.5	117.4
3.84	473	0.2364	0.4016	0.8848	89.09(3)	6.265	7.49	4.41	189.0	121.8
3.36	308	0.2340	0.3946	0.8840	88.76(3)	6.288	7.56	4.48	191.1	126.2
2.94	303	0.2352	0.3954	0.8851	88.95(4)	6.275	7.53	4.48	187.9	125.9
4.92	1073	0.2450	0.4258	0.8931	90.76(4)	6.150	7.29	4.20	182.2	108.5
4.43	873	0.2424	0.4172	0.8896	90.25(5)	6.185	7.34	4.26	183.6	112.2
3.89	673	0.2402	0.4102	0.8878	89.77(4)	6.217	7.39	4.33	184.1	116.6
3.20	473	0.2382	0.4038	0.8859	89.40(3)	6.243	7.44	4.39	185.2	120.3
2.82	308	0.2358	0.3964	0.8849	89.02(4)	6.270	7.51	4.46	187.3	124.7
2.36	303	0.2372	0.3976	0.8858	89.23(5)	6.255	7.47	4.46	183.1	124.4
3.84	873	0.2446	0.4206	0.8897	90.56(5)	6.163	7.27	4.23	178.7	110.3
3.35	673	0.2422	0.4132	0.8891	90.06(4)	6.198	7.34	4.30	181.1	114.6
2.67	473	0.2400	0.4060	0.8864	89.68(3)	6.224	7.39	4.37	181.4	118.9
2.05	308	0.2378	0.3986	0.8851	89.41(4)	6.243	7.44	4.44	181.5	123.1
1.85	303	0.2390	0.4008	0.8860	89.49(4)	6.237	7.41	4.42	180.0	121.8
3.12	873	0.2466	0.4236	0.8918	90.96(4)	6.136	7.23	4.21	175.7	108.8
2.65	673	0.2442	0.4164	0.8896	90.43(3)	6.172	7.29	4.27	178.0	112.5
2.06	473	0.2422	0.4102	0.8872	89.99(3)	6.202	7.33	4.33	178.2	116.3
1.50	308	0.2400	0.4024	0.8855	89.68(3)	6.224	7.38	4.40	178.3	120.5
0.77	303	0.2420	0.4066	0.8877	90.05(5)	6.198	7.34	4.37	176.1	118.4
1.98	673	0.2466	0.4210	0.8909	90.80(5)	6.147	7.23	4.23	174.7	110.0
1.35	473	0.2446	0.4148	0.8895	90.37(5)	6.176	7.27	4.29	174.8	113.7
0.96	308	0.2422	0.4070	0.8877	89.97(4)	6.204	7.33	4.36	176.1	117.9

Notes: Pressure on sample calculated using Equation 14. Values in parentheses are 1σ error in the last digits. Two-way travel times have 1σ of ~0.4 ns for S waves and ~0.2 ns for P waves. The precision of image measurement of sample length is 0.2–0.4%. Uncertainties in velocities are less than 0.3%, and less than 1.0% for the derived elastic moduli. The densities at high pressures are calculated using unit-cell volumes obtained from X-ray diffraction.

TABLE 2. Comparison of thermoelastic properties of ε-FeSi

Ref.	V_0 (Å³)	*K* (GPa)	*K*′	∂*K*/∂*T* (GPa/K)	*G* (GPa)	*G*′	∂*G*/∂*T* (GPa/K)	Notes
1*	90.45(3)	168.9(7)	6.6(2)	–0.023(1)	116.5(3)	2.9(1)	–0.030(1)	UI–X; 8 GPa, 1273 K
2*	90.45(3)	169.3(8)	6.5(3)	–	116.3(4)	3.0(1)	–	UI–X; 12 GPa, 300 K
3*	–	173‡	–	–	116‡	–	–	RUS; 50–380 K
4†	89.015	209	3.5	–	–	–	–	EoS; 50 GPa, RT
5†	90.21(2)	160	4§	–	–	–	–	NToF EoS; 9 GPa, RT
6†	90.39(4)	172	4§	–0.043	–	–	–	EoS; 8.25 GPa, RT
7†	90.193	184.7	4.75	–	–	–	–	EoS; 50.7 GPa, RT
8*	88.896	227	3.9	–	–	–	–	Calc.; 0 K
9	84.090	255	4.143	–	–	–	–	Calc.; LDA
9	90.174	221	4.175	–	–	–	–	Calc.; GGA

Notes: UI-X = ultrasonic interferometry w/ X-ray; RUS = resonant ultrasonic spectroscopy; EoS = equation of state (static compression); NToF = neutron time-of-flight. References: 1 = this study; 2 = Whitaker et al. (2008); 3 = Sarrao et al. (1994); 4 = Knittle and Williams (1995); 5 = Wood et al. (1995); 6 = Guyot et al. (1997); 7 = Lin et al. (2003); 8 = Vocadlo et al. (1999); 9 = Caracas and Wentzcovitch (2004).

* Adiabatic values.

† Isothermal values.

‡ Estimates based on graphical data.

§ Assumed value.

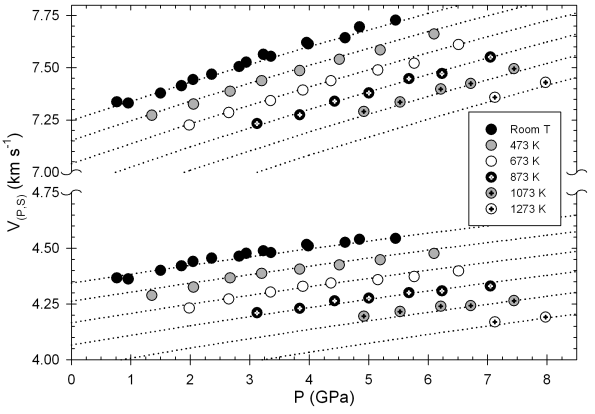

FIGURE 2. Variation of elastic compressional (v_P) and shear (v_S) wave velocities for ε-FeSi as a function of pressure and temperature from the ultrasonic measurements and X-ray data to 8 GPa and 1273 K. Data above the break are P-wave velocities, and data below the break are S-wave velocities. Data symbols are coded by temperature as shown in the legend; velocities obtained from the finite-strain fitting of the thermoelastic data are shown as dashed lines.

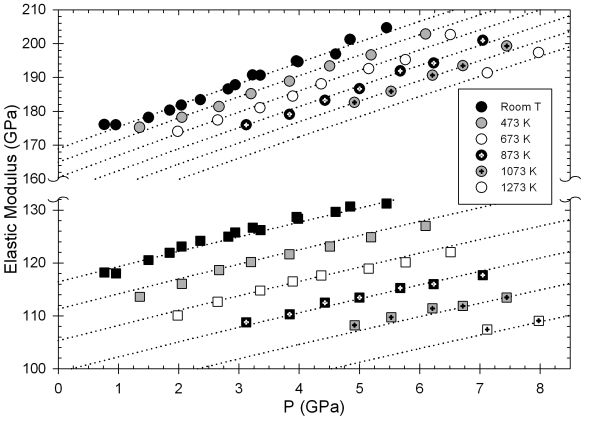

FIGURE 3. Variation of experimental measurements of elastic bulk (K_S) and shear (G) moduli as a function of pressure. Circles are adiabatic bulk modulus measurements, squares are shear modulus values; symbols are coded by temperature, using the same coding for both elastic moduli. The third-order finite-strain fits of these experimental data are shown as dashed lines.

X-rays or neutrons to determine the cell volume of the material at that pressure. This pressure and volume data were then fit to an equation of state to determine K_{T0} and K_{T0}'. This means the parameters obtained from this fitting are heavily dependent upon the accuracy of the pressure measurement. In addition, fixing the value of one of these parameters can dramatically change the other, as in the fitting procedure K_{T0} and K_{T0}' are strongly correlated with each other as well as with the volume at zero pressure. For instance, the compression curve (V/V_0 vs. P) derived using the equation of state parameters (K_{T0}, K_{T0}', and V_0) of Lin et al. (2003) are found to be in agreement within 0.3% with that obtained from the current study up to their highest pressure (50.7 GPa), but the apparent values of K_{T0} and K_{T0}' differ from the current study as much as 12 and 28%, respectively (Table 2; see also Whitaker et al. 2008). The advantage of the study reported here over the previously reported studies is twofold. First, at each set of pressure and temperature conditions, we directly measure the bulk and shear modulus, rather than relying on fitting of volume data alone, and this leads to a more reliable and complete data set. Second, the results obtained using these techniques are not dependent upon any external pressure calibration based on a standard. These two factors combine to give an inherently robust and internally consistent data set that cannot be obtained using individual X-ray diffraction or acoustic methods.

This study has helped to further resolve some existing controversy regarding the elastic properties of ε-FeSi by providing the first complete set of thermodynamically internally consistent elastic moduli and their first pressure and temperature derivatives. The results presented here will allow the refinement of existing models and calculations involving this phase by providing new constraints on its behavior at high pressure and temperature. The data presented here, along with studies currently underway on other iron silicide alloys, will be of great help in determining the possible presence of Si in the Earth's core.

ACKNOWLEDGMENTS

The authors gratefully acknowledge the constructive reviews of J. Zhang, H. Terasaki, and G.D. Gatta that helped to improve this manuscript. This research is supported by NSF grants EAR00135550 and EAR0635860 to B.L. Use of the National Synchrotron Light Source, Brookhaven National Laboratory, was supported by the U.S. Department of Energy, Office of Science, Office of Basic Energy Sciences, under Contract no. DE-AC02-98CH10886. Use of the X17B2 beamline was supported by COMPRES, the Consortium for Materials Properties Research in Earth Sciences under NSF Cooperative Agreement EAR 01-35554 and by the Mineral Physics Institute, Stony Brook University. MPI Publication no. 475.

REFERENCES CITED

Badro, J., Fiquet, G., Guyot, F., Gregoryanz, E., Occelli, F., Antonangeli, D., and d'Astuto, M. (2007) Effect of light elements on the sound velocities in solid iron: Implications for the composition of Earth's core. Earth and Planetary Science Letters, 254, 233–238.

Caracas, R. and Wentzcovitch, R. (2004) Equation of state and elasticity of FeSi. Geophysical Research Letters, 31, L20603.

Davies, G.F. and Dziewonski, A.M. (1975) Homogeneity and constitution of Earth's lower mantle and outer core. Physics of the Earth and Planetary Interiors, 10, 336–343.

Dziewonsky, A.M. and Anderson, D.L. (1981) Preliminary reference Earth model. Physics of the Earth and Planetary Interiors, 25, 297–356.

Georg, R.B., Halliday, A.N., Schauble, E.A., and Reynolds, B.C. (2007) Silicon in the Earth's core. Nature, 447, 1102–1106.

Guyot, F., Zhang, J.H., Martinez, I., Matas, J., Ricard, Y., and Javoy, M. (1997) *P-V-T* measurements of iron silicide (epsilon-FeSi). Implications for silicate-metal interactions in the early Earth. European Journal of Mineralogy, 9, 277–285.

Jephcoat, A. and Olson, P. (1987) Is the inner core of the Earth pure iron? Nature, 325, 332–335.

Knittle, E. and Williams, Q. (1995) Static compression of ε-FeSi and an evaluation of reduced silicon as a deep Earth constituent. Geophysical Research Letters, 22, 445–448.

Li, B.S. and Zhang, J.Z. (2005) Pressure and temperature dependence of elastic wave velocity of $MgSiO_3$ perovskite and the composition of the lower. Physics of the Earth and Planetary Interiors, 151, 143–154.

Li, B.S., Chen, K., Kung, J., Liebermann, R.C., and Weidner, D.J. (2002) Sound velocity measurement using transfer function method. Journal of Physics: Condensed Matter, 14, 11337–11342.

Li, B.S., Kung, J., and Liebermann, R.C. (2004) Modem techniques in measuring elasticity of Earth materials at high pressure and high temperature using ultrasonic interferometry in conjunction with synchrotron X-radiation in multi-anvil apparatus. Physics of the Earth and Planetary Interiors, 143–144, 559–574.

Lin, J.F., Campbell, A.J., Heinz, D.L., and Shen, G.Y. (2003) Static compression of iron-silicon alloys: Implications for silicon in the Earth's core. Journal of Geophysical Research: Solid Earth, 108, 2045.

Liu, W., Kung, J., and Li, B.S. (2005) Elasticity of San Carlos olivine to 8 GPa and 1073 K. Geophysical Research Letters, 32, L16301.

Mao, H.K., Shu, J.F., Shen, G.Y., Hemley, R.J., Li, B.S., and Singh, A.K. (1998) Elasticity and rheology of iron above 220 GPa and the nature of the Earth's inner core. Nature, 396, 741–743.

McDonough, W.F. and Sun, S.S. (1995) The composition of the Earth. Chemical Geology, 120, 223–253.
Pauling, L. and Soldate, A.M. (1948) The nature of the bonds in the iron silicide FeSi and related crystals. Acta Crystallographica, 1, 212–216.
Sarrao, J.L., Mandrus, D., Migliori, A., Fisk, Z., and Bucher, E. (1994) Elastic properties of FeSi. Physica B, 199, 478–479.
Vocadlo, L., Price, G.D., and Wood, I.G. (1999) Crystal structure, compressibility and possible phase transitions in ε-FeSi studied by first-principles pseudopotential calculations. Acta Crystallographica Section B: Structural Science, 55, 484–493.
Vocadlo, L., Knight, K.S., Price, G.D., and Wood, I.G. (2002) Thermal expansion and crystal structure of FeSi between 4 and 1173 K determined by time-of-flight neutron powder diffraction. Physics and Chemistry of Minerals, 29, 132–139.
Whitaker, M.L., Liu, W., Liu, Q., Wang, L., and Li, B. (2008) Combined in situ synchrotron X-ray diffraction and ultrasonic interferometry study of ε-FeSi at high pressure. High Pressure Research, 28, 385–395.
Wood, I.G., Chaplin, T.D., David, W.I.F., Hull, S., Price, G.D., and Street, J.N. (1995) Compressibility of FeSi between 0 and 9 GPa, determined by high-pressure time-of-flight neutron powder diffraction. Journal of Physics: Condensed Matter, 7, L475–L479.

Manuscript received December 5, 2008
Manuscript accepted February 20, 2009
Manuscript handled by G. Diego Gatta